Journal of Materials Chemistry B

Accepted Manuscript

ROYAL SOCIETY OF CHEMISTRY

www.rsc.org/materialsB

Cite this: DOI: 10.1039/c0xx00000x

www.rsc.org/xxxxxx

ARTICLE TYPE

The studies on high concentrated complex dispersions of gold nanoparticles and temperature-sensitive nanogels and their application as new blood-vessel-embolic materials with high-resolution angiography

Yingying Ma,[a] Jiangshan Wan,[a] Kun Qian,[b] Shinan Geng,[a] Nijun He[a], Guofeng Zhou[b], Yanbing Zhao*[a] and Xiangliang*[a]

Received (in XXX, XXX) Xth XXXXXXXXX 20XX, Accepted Xth XXXXXXXXX 20XX
DOI: 10.1039/b000000x

Recently temperature sensitive polymers have been developed as novel embolization materials. However, their flowability and embolization have been seriously impacted by iodine-based X-ray contrast agents. In order to resolve the drawbacks of these contrast agents, high concentrated complex (HCC) dispersions of gold nanopaticles (GNPs) with p(*N*-isopropylacrylamide-*co*-butyl methylacrylate) (PIB) nanogels were developed as new blood-vessel-embolic materials with high-resolution angiography. Although GNPs have better X-ray attenuation than iodinated compounds, their poor dispersion stability limits the application in digital subtraction angiography (DSA). HCC dispersions show excellent X-ray attenuation ability which is 2.6 times higher than Omipaque at 0.31 mol/L. It can be attributed to the fact that the sol-gel transition of nanogel dispersions improves the colloid stability of GNPs. In two sol-gel transitions temperature ($T_{g\text{-}s}$ and $T'_{s\text{-}g}$) of nanogel dispersions, GNPs have no influence on the $T'_{s\text{-}g}$, and great influence on the $T_{g\text{-}s}$. The *in vivo* experimental data indicate that HCC dispersions show high angiographic ability and good blood-vessel embolization, and can be used to postoperative examination for long periods owing to the entrapment of GNPs into the embolic sites. The HCC dispersions are hopeful to be developed as new blood-vessel-embolic materials with high-resolution angiography.

Introduction

Transcatheter Arterial Embolization (TAE), an image-guided locoregional therapy, plays an increasingly important role in interventional radiology.[1,2] By using embolic materials to occlude blood flow, it has been widely applied in the treatment of various diseases, such as tumors, arteriovenous malformations, aneurysms and hemorrhages.[3] The therapeutic effect of TAE was highly dependent on the properties of these embolic materials. Specifically in the TAE treatment of tumors, an ideal embolic agent must meet various requirements including good flowability in fine catheter, efficient embolization to blood-vessels, high resolution in angiography and good biocompatibility.[4,5]

Although many materials including cyanoacrylate polymers, polyvinyl alcohol (PVA) microparticles, ethylene (vinyl alcohol), Lipiodol®/Lipiodol Ultra-Fluide® *etc*. has been extensively used, there are several hazards in their clinical application. For example, ethylene (vinyl alcohol) (ONYX®) needs to be dissolved in toxic organic solvents (e.g. dimethyl sulfoxide) for delivery,[6] and water-based embolic materials (e.g. cyanoacrylate polymers) can suffer from drawbacks such as adhesion to catheter and monomer toxicity.[7] Although PVA microparticles and other polymer microspheres showed excellent permanent embolization owing to their mechanical strength in TAE therapy, it is difficult for them to pass through a microcather (due to poor flowability) and move into the peripheral arteries of solid tumors (due to relatively large size).[8,9] On the other hand, Lipiodol®/Lipiodol Ultra-Fluide®, which has good flowability, can move rapidly into the peripheral arteries of tumors. However, its lower embolic strength leads to its rapid elimination under blood scouring, and this results in vascular recanalization in tumor tissue.[10]

In our previous research,[11] the temperature sensitive nanogels have been developed as novel blood-vessel-embolic materials in the interventional therapy of hepatocellular carcinoma. The dilemma between flowability and embolization in clinical embolic agents has been resolved well by using the temperature sensitive sol-gel phase transition of p(*N*-isopropylacrylamide-*co*-butyl methylacrylate) (PIB) nanogels. In order to monitor the blood-vessel embolization of PIB nanogels, high concentration of X-ray contrast (iondinated compounds such as Omnipaque) must be combined with PIB nanogels for the image-guided embolization therapy in clinic. Owing to the strong influence of these iondinated compounds on the temperature sensitive sol-gel behavior, the operative procedures of blood-vessel embolization with PIB nanogels were complicated, and then increased the difficulty and hazard of the operations. In addition, these small-molecular contrasts allow only very short imaging times due to rapid clearance by the kidney. Therefore, it was difficult to evaluate postoperative efficacy by imaging examinations for long periods. Moreover, iodinated contrast media was limited to use in

many patients due to their iodine allergy.

Gold nanoparticles (GNPs) have been used widely in diagnosis and therapeutics over the past decade due to their excellent electronic, optical and thermal properties.[12,13] Recently great attentions have been paid for GNPs as a computed tomography (CT) contrast agent due to their higher X-ray absorption coefficient, longer imaging time and better biocompatibility than iodine-based contrast agents.[14-17] In the interventional therapy and diagnosis of tumors, digital subtraction angiography (DSA) has been widely, and required higher concentration of X-ray contrast agents owing to its lower X-ray energy and resolutions compared to CT. Unfortunately, the heavy aggregation of GNPs at high concentration has greatly limited their application in the DSA imaging due to their lack of sufficient stability. In order to improve the colloid stability of GNPs, some hydrophilic macromolecules (*e.g.* PEG and dendrimers) were synthesized for the surface-modification on GNPs.[18,19] The resultant GNPs exhibited great potential as a CT contrast agents in blood-pool imaging.[20]

In order to resolve the drawbacks of iodine-based contrast agent in blood-vessel embolization therapy of temperature sensitive nanogels, some groups were engaged to develop iodine-based macromolecules as CT contrast agents.[21,22] In our present work, high concentrated complex (HCC) dispersions between temperature sensitive nanogels and GNPs are developed as novel blood-vessel-embolic materials with high-resolution angiography. The temperature sensitive nanogels can improve the DSA imaging ability of HCC dispersions since the gellation of nanogel dispersions can greatly inhibit the aggregation of GNPs. In addition, the GNPs in HCC dispersions can stay at the embolism sites for long periods. It can provide an opportunity to evaluate long-term efficacy of embolization therapy using DSA examination. On the other hand, GNPs can increase the gellation strength of temperature sensitive nanogels, and then improve the TAE therapic efficacy. To our knowledge, this is the first report about high concentrated complex (HCC) between temperature sensitive nanogels and GNPs as blood-vessel-embolic materials with high-resolution angiography.

Experimental

Reagents

Hydrogen tetrachloroaurate (III) hydrate ($HAuCl_4 \cdot xH_2O$, Au content > 47.8%, Sinopharm Chemical Reagent Co., Ltd., China), trisodium citrate dehydrate (purity > 99.0%, Tianjin University Chemical Reagent Co., Ltd., China), Gold standard solution (1000 μg/mL, Aladdin Reagent Co., Ltd., China), Sodium dodecyl sulfate (SDS, purity ≥ 86.0%, Kermel Chemical Industry Co., Ltd., China) and potassium persulfate (KPS, purity ≥ 99.5%, Kermel Chemical Industry Co., Ltd., China) were used as received. *N*-isopropylacrylamide (NIPAM, purity > 98.0%, Tokyo Chemical Industry, Japan) and *N,N′*-methylene-bisacrylamide (BIS, purity > 99.0%, Kermel Chemical Industry, China) were recrystallized from *n*-hexane and methanol, respectively. Butyl methylacrylate (BMA, purity > 99.5%, Kermel Chemical Reagent Co., Ltd., China) was distilled before use. Iohexol (Omnipaque, a nonionic radiopaque agent) and PVA foam embolization particles (Ivalon, 180-300 μm) was purchased from B.Braun Melsungen AG (Germany) and Cook Medical (USA), respectively. Milli-Q Ultrapure water (18.2 MΩ) was used in all experiments. All glassware used in the experiments was washed with "aqua regia" (1:3, concentrated nitric acid / concentrated hydrochloric acid) and rinsed with ethanol and ultrapure water. Japanese rabbits (*ca*. 3 kg weight, both sexes) were provided by Laboratory Animal Research Center, Tongji Medical Institute of Huazhong University of Science and Technology. All procedures were in accordance with China National Animal Law on the use of laboratory animals.

The preparation of concentrated gold nanoparticle (cGNP) dispersions

Gold nanoparticles (φ15 nm) were synthesized by a modified citrate reduction method (Frens method).[23] Briefly, 92 mL of freshly prepared $HAuCl_4$ (0.1 mmol/L) solution was refluxed in a 250 mL three-necked flask while stirring. Afterwards, 8 mL of sodium citrate solution (59.5 mmol/L) was quickly added as both reducing agent and capping agent. The orange color of Au^{3+} ion disappeared rapidly (*ca.* 15 s) owing to the reduction of Au(III) to Au(I), and then turned into black subsequently since Au(I) ions were further reduced to small seeds of zero-valent gold particles. The black color of the gold seeds turned further into burgundy gold nanoparticle dispersion in 2 minutes. After the reaction was maintained under the same condition for another 15 minutes, the gold nanoparticle dispersion was cooled to room temperature. 15 mL of the gold nanoparticle dispersions were added in a centrifugal filter (Millipore's Amicon® Ultra-15, molecular weight cutoff 100,000 Da), and then centrifuged (3000 rpm) for 10 minutes by the ultrafiltration centrifugation method. After removal of the filtrate solution, the concentrated gold nanoparticle (cGNP) dispersion was obtained and stored in 4 °C. The gold content in cGNP dispersion was 0.04 mol/L by the determination of an inductively coupled plasma source mass spectrometer (ICP-MS). The mean diameter of gold nanoparticles was 15 ± 2 nm characterized by a transmission electron microscope (TEM).

The preparation of p(*N*-isopropylacrylamide-*co*-butyl methylacrylate) (PIB) nanogels

p(*N*-isopropylacrylamide-*co*-butyl methylacrylate) (PIB) nanogels were prepared using precipitation polymerization as previously reported.[11] Briefly, NIPAM (2.26 g, 20mmol), BMA (0.17 mL，1.0mmol), BIS (32.4 mg, 0.2mmol) and SDS (32 mg, 0.65 mmol) were dissolved in 170 mL of ultrapure water in a three-necked flask equipped with a reflux condenser, a gas inlet and a thermometer. While stirring, the solution was degassed for at least 60 min by bubbling N_2 and heating to 70 °C. Afterwards, KPS (95 mg, 0.35 mmol) was then added rapidly as an initiator. After the polymerization was maintained under an N_2 atmosphere at 70 °C for 4.5 h, the resultant PIB nanogel dispersion was dialyzed (the cutoff molecular weight is 14000) against water for 2 weeks to remove un-reacted monomers and other small molecules. 10 mL of the dialyzed dispersion was withdrawn for the hydrodynamic diameter determination using dynamic light scattering technology. The rest of the nanogel dispersion was lyophilized and stored in a desiccator at room temperature.

The high concentrated complex (HCC) dispersions of PIB nanogels and cGNPs

The high concentrated complex (HCC) dispersions with various concentrations of PIB nanogels and cGNPs were prepared according to the formulation in table 1. For example, 40 mg lyophilized powder of PIB nanogels was added to 7 mL of cGNP dispersion, and stirred overnight for swelling adequately. The resultant dispersion was frozen rapidly using liquid nitrogen in order to avoid the aggregation and precipitation of gold nanoparticles in a slowly-freezing process. After lyophilized the frozen dispersion, the freeze-dried powder was re-dissolved in 1 mL of ultrapure water, while stirring overnight. The resulting HCC dispersions with good dispersion stability was denominated as HCC431, in which the first number, 4, indicated 4 wt% of nanogel concentration, and the last two numbers, 31, indicated 0.31 mol/L of gold content in the HCC dispersion.

Characterization

UV-Vis absorption spectra of gold nanoparticle dispersions were collected with a Shimadzu UV-1750 dual-beam spectrophotometer in the 400 - 800 nm range at room temperature. PCG and HCC dispersions were diluted to ca. 0.01 - 0.03 mg/mL of Au concentration for the UV-Vis determinations with 1 cm path length quartz cuvettes. The gold element in cGNP and HCC dispersions was measured using an inductively coupled plasma source mass spectrometer (ICP-MS, ELAN DRC-e, PerkinElmer, USA). The reference solutions with various concentrations (10 ppb, 20 ppb, 50 ppb and 100 ppb) were prepared using a gold standard solution (GSB04-1715-2004), and the sample solutions were diluted to less than 100 ppb. The hydrodynamic diameters and the zeta potentials of PIB nanogels were determined by dynamic light scattering (DLS, Zetasizer Nano ZS90, Malvern Instrument Ltd., Worcestershire, UK) equipped with a 4 mW He-Ne laser source (λ = 633 nm) with a scattering angle of 90°. All samples were diluted with ultrapure water to 0.5 mg/mL. The hydrodynamic diameters and the zeta potentials were measured at the various temperatures from 25 °C to 45 °C with pre-equilibration for at least 10 min at each point. The size and morphology of PIB nanogels and gold nanoparticles were characterized on a transmission electron microscope (TEM, JEM-2010, JEOL, Tokyo, Japan) at 200 kV. PIB nanogel and gold nanoparticles dispersions were dropped onto carbon film-coated 300-mesh TEM copper grids for 15 min. Afterwards, PIB nanogels were stained using a drop of phosphotungstic acid (5%, w/v). The samples were dried at room temperature. The gellating microstructure of HCC dispersions was characterized using a scanning electron microscope (SEM, Nova NanoSEM 450, FEI, Netherlands) at 10.00 KV. Sample dispersions were rapidly frozen by liquid nitrogen, and then lyophilized in order to protect their microstructures from being destroyed. The crystal structure of gold nanoparticles was studied by X-ray diffraction (XRD) on a diffractometer (X'Pert PRO, PANalytical B. V., Almelo, the Netherlands) using Cu Kα radiation at λ = 0.1541 nm and operating at 40 kV and 40 mA. Patterns of each sample were recorded from 10° to 90° with a step size of 0.0167° and a step time of 7.620 s

X-ray attenuation evaluation

100 μL of HCC dispersions and iohexol 300 (Omnipaque, 300 mg I/mL, B.Braun Melsungen AG) with various concentrations were prepared respectively into 2 mL glass vials, and then placed in a scanning holder. Dynamic contrast-enhanced CT scans were performed using a CT scanner (somatom sensation 64 spiral, Siemens) with 100 kV, 120 mA and body PCT mode. The contrast enhancement of HCC dispersions and Omnipaque was measured using a standard display program in Hounsfield units (HU) for each concentration of HCC dispersions and Omnipaque. The X-ray mode of IVIS Lumina XR system (Caliper Life Sciences, Hopkinton, USA) was also used for the X-ray attenuation determination of HCC dispersions and Omnipaque. 100 μL of HCC dispersions and Omnipaque with various concentrations were added into a 96-well plate, and the entire region of a well was selected as the region of interest (ROI) for the sample in the well. The gray value of ROI was measured using the built-in living imaging® software for the X-ray attenuation evaluation.

The sol-gel transition behavior of HCC dispersions

The temperature sensitive sol-gel transition behavior of HCC dispersions was determinated by inverting-vial method at various temperatures from 4 °C to 37 °C. The samples were maintained for 5 min at each temperature point before determination. The dynamic viscoelastic properties of HCC dispersions were measured using a stress-controlled rheometer (Kinexus ultra+, Malvern Instrument Ltd. UK) with a parallel plate (PP50, Φ = 50 mm, the gap set at 0.5 mm) in the temperature range of 20 °C - 45 °C with following parameters: The stress was 0.05 Pa, the heating rate was 1 °C min^{-1}, and the frequency was 1.0 Hz.

Animal study

The blood-vessel embolization with HCC dispersions was performed on the right renal of Japanese big ear rabbit. After abstained from eating and drinking for 12 h, fifteen of normal rabbits were anesthetized by intravenous administration of 30 mg kg^{-1} of pentobarbital sodium (Sigma) into their auricular veins. The rabbits were fixed in the supine position as pain disappeared in 5-10 min. Their groin skins were dissected, and the femoral arteries were separated using ophthalmic forceps. After the distal arteries ligation, a 4F coaxial microcatheter was introduced into the proximal arteries by an 18 G puncture needle. The angiographies of rabbit renal arteries were firstly performed by injecting a contrast agent (Omnipaque, 300 mg I/mL) at an injecting rate of 0.5 mL/s. Afterwards, the HCC dispersions were injected at the injecting rate of 0.4 mL/s, and 10 minules later, the angiographies of the renal arteries were performed again for the examination of embolization. All of these interventional operations were guided using digital subtraction angiography (DSA, Siemens Bicor Top., Germany) under aseptic condition. The embolic efficacy was assessed histopathologically and angiographically at various time points after embolization. Moreover, 4 mL of blood was collected from the femoral artery of Japanese big ear rabbit at various times after embolization, and sent to the clinical laboratory of Huazhong University of Science and Technology Hospital for the hepatorenal function analysis immediately

Biocompatibility evaluation

Cytotoxicity test: 0.5 mL of HCC dispersions or PIB nanogels (8 wt%) was added in a 24-well plate, and 1.6 mL of DMEM

medium was added after gellation occurred at 37 °C. The DMEM solutions were collected as the extracting solutions of HCC dispersions after incubated at 37 °C for 24h. The cytotoxicity of HCC dispersions was evaluated by Cell Counting Kit-8 (CCK-8). In brief, mouse embryonic fibroblasts cell strain (L929 cells, 5×10^4/mL) were seeded in 96-well plates at 100 μL/well. When the cells overspread 80-85% of a well area, the extracting solutions were added, and DMEM medium was added as negative control. The blank control was the DMEM medium without cells. 10 μL of CCK-8 reagent (Dojindo China CO., Ltd, Japan) were added in each well after 3 days of incubation at 37°C, and was incubated further for 3h. Optical density (OD value) was examined by a microplate reader (1420 multilabel counter, Perkin Elmer, MA, USA) at the measuring wavelength of 450 nm. Cell viability (CV) was calculated by the following equation:

$$\mathrm{CV} = (\mathrm{OD_h} - \mathrm{OD_b})/(\mathrm{OD_n} - \mathrm{OD_b}) \times 100\%.$$

Here, OD_h, OD_b and OD_n were the OD value of HCC dispersion groups, blank control groups and negative control groups, respectively.

The hemolysis test: Red cell suspension (RCS) was obtained through centrifugation (1500 rpm×10 min, repeated three times) of the mixing solution of rat whole blood and normal saline. 150 μL of HCC dispersions and/or PIB nanogels was added in a centrifuged tube (1.5 mL), and incubated at 37 °C for 5 min. The supernatant was collected by centrifugation (3000 rpm×10 min) after 150 μL of RCS was added and incubated at 37 °C for 1 h. Pure water and normal saline were positive control and negative control, respectively. the optical density (OD value) was examined by a microplate reader (1420 multilabel counter, Perkin Elmer, MA, USA) at the measuring wavelength of 540 nm. Hemolysis ratio (*Hr*) was calculated by the following equation:

$$Hr = (\mathrm{OD_h} - \mathrm{OD_n})/(\mathrm{OD_p} - \mathrm{OD_n}) \times 100\%.$$

Here, OD_h, OD_p and OD_b were the OD value of HCC dispersion or PIB nanogel groups, positive control groups and negative control groups, respectively.

Result and Discussion

The Preparation and Characterization of Gold nanoparticles and PIB nanogels

The gold nanoparticles (GNPs) with high homogeneity were prepared by modified citrate reduction,[23] and their meaning size was *ca.* 15 ± 2 nm according to the TEM imaging in Figure 1A. Through adjusting the molar ratio of feeding sodium citrate and $HAuCl_4$ in our experiments, near monodisperse GNPs could be tailored in the size range of 12 – 150 nm. In according with previous reports[24], the XRD data in Figure 1B indicated the four diffraction peaks at 2θ = 38, 44, 65 and 78 was responding respectively to the four crystal facets of the GNPs: {111}, {200}, {220} and {311}. Temperature sensitive p(*N*-isopropylacrylamide-*co*-butyl methylacrylate) (PIB) nanogels was synthesized as reported previously.[11] Similarly with the previous reports, the hydrodynamic diameter of PIB nanogels was about 211 nm at 20 °C , and decreased to 77 nm at 40 °C, about a reduction of 2.74 times in size and 20 times in volume. As shown in Figure 2, the zeta potential of PIB nanogels increased from -7.7 mV to -22.3 mV when temperature increased from 24 °C to 45 °C, a *ca.* 2.9 fold increase. TEM photograph (Figure 2B) showed that PIB nanogels were spherical hydrogel particles with good homogeneity. Their sizes were about 200 nm at room temperature in according with the determination by DLS technology. Since the crosslinking density of nanogel core was possibly higher than that of nanogel surface,[25] the core-shell structures composed with the dense cores and the loosen shells was found in the inset plot of Figure 2.

The Colloid Stability of HCC Dispersions

Compared with X-ray computed tomography (CT) with better spatial resolution, digital subtraction angiography (DSA) need higher concentration of gold nanoparticle contrast agent in order to realize clinical angiography To avoid the aggregation of gold nanoparticles, concentrated gold nanoparticle (cGNP) dispersions (0.04 mol/L) were obtained firstly through an ultrafiltration of the GNP dispersions (*ca.* 0.1 mg Au/mL) prepared citrate reduction methods, and mixed quickly with PIB nanogels. After lyophilized, the as-prepared powders of the mixtures (HCC431) remained the characteristic color (burgundy) of the gold nanoparticles. As shown in the inset photographs of Figure 3A, however, a dense precipitation with black color was formed for the lyophilized powders of the cGNP dispersions without PIB nanogels. The characteristic UV/Vis peaks (λ = 520 nm) of gold nanoparticles disappeared completely since the lyophilized powders of the cGNP dispersions could be hardly re-dispersed in water (Figure 3B). The lyophilized powders of HCC431, by contrast, dispersed easily in water (Figure 3C). The resulting HCC431 dispersions showed the similar UV/Vis peaks (λ = 524 nm) of gold nanoparticles, although a slight red-shift was found (Figure 3A). The SEM photographs in Figure $3D_1$-$3D_4$ also indicated that PIB nanogels could prevent effectively the aggregation of gold nanoparticles. A fibrous networks was formed by PIB nanogels (Figure $3D_1$). Being attached onto the surface of the fibrous 3D networks, Most of the gold nanoparticles in HCC431 (0.31 mol/L) remained good dispersibility (Figure $3D_2$). Although the gold content in cGNP dispersions (0.04 mol/L) was much lower than HCC dispersions, almost all of gold nanoparticles aggregated to form large precipitation, and few of individual gold nanoparticles were found in Figure $3D_3$. In sharp contrast, all of gold nanoparticles had great dispersibility in HCC dispersions as shown in Figure $3D_4$. These data indicated that PIB nanogels played a key role on improving the dispersion stability of the gold nanoparticles in HCC dispersions.

The X-ray attenuation of HCC Dispersions

The X-ray attenuation of HCC dispersions was examined on a CT scanner and an IVIS Lumina XR system (X-ray determination model). As shown in Figure 4A, the X-ray attenuation of HCC dispersions increased linearly with the increasing of gold concentration. The Hounsfield unit (Hu) of HCC dispersions increased from 573.6 of 0.09 mol Au/L to 2150.2 of 0.31 mol Au/L, while that of Omipaque, a commercial iodinated contrast agent, increased linearly from 392.5 of 0.14 mol I/L just to 1190.7 of 0.48 mol I/L. This means that the X-ray attenuation of HCC dispersions was 2.6 times higher than Omipaque at 0.31 mol/L(2150 Hu *vs* 823 Hu). Likewise, the gray value of HCC dispersions increased from 0.8×10^6 of 0.09 mol Au/L to 1.8×10^6 of 0.31 mol Au/L in the X-ray determination of IVIS Lumina XR system (Figure 4B), while that of Omipaque increased from

0.8×10^6 of 0.31 mol I/L to 1.0×10^6 of 0.48 mol I/L. These results clearly indicated that owing to their good dispersion stability, HCC dispersions exhibited a much higher X-ray attenuation than Omipaque at the same concentration, and had a great potential for used as blood-pool contrast agent.

The sol-gel phase transition of HCC Dispersions

The temperature sensitive transition behavior of HCC dispersions was shown in Figure 5. Similarly with PIB nanogels reported previously by us,[11] HCC dispersions also exhibited three phase states: Swollen gel (Phase 1), flowable sol (Phase 2) and shrunken gel (Phase 3). Two phase transition temperatures ($T_{g\text{-}s}$ and $T'_{s\text{-}g}$) were corresponding respectively to the transition from swollen gel to flowable sol and the transition from flowable sol to shrunken gel. As shown in Figure 5A, the $T_{g\text{-}s}$ values of HCC dispersions increased with the increasing concentraion of PIB nanogels. According to hardsphere theory,[26,27] the increasing $T_{g\text{-}s}$ could be attributed to the volume blocking effect with the increase of the nanogel concentration. However, the transition from flowable sol to shrunken gel resulted from the enhanced inter-particle interactions (hydrophobic attraction and electrostatic repulsion) which were independent of nanogel concentration. Therefore, the $T'_{s\text{-}g}$ values had remained virtually unchanged whether the nanogel concentration changed or not (Figure 5A and 5B).

Similarly, gold nanoparticles had little impact on the $T'_{s\text{-}g}$ values of HCC dispersions (Figure 5B). The $T_{g\text{-}s}$ values, however, increased at first and decreased afterwards with the increasing concentration of gold nanoparticles. The maximum $T_{g\text{-}s}$ appeared at about 40 mg Au/mL of Au content. The reduced $T_{g\text{-}s}$ above 40 mg Au/mL might be attributed to the decreasing of volume fraction of PIB nanogels since it could be reasonable to assume that a large amount of Au nanoparticles led to the decrease in the sizes of PIB nanogels.

Similarly with the results from Figure 5, the viscoelastic properties of HCC431 dispersions also exhibited three phases (swollen gel, flowable sol and shrunken gel) in the storage modulus (G') and loss modulus (G") changes with temperature (Figure 6A). As temperature increased, the G' and G" values of HCC431 and PIB nanogel dispersions decreased, and the phase transition from swollen gel to flowable sol occurred when the gel strength further decreased as temperature increased to about 26–30 ^{o}C. Owing the reduction in the size of PIB nanogels with temperature, the volume fraction of HCC and PIB nanogel dispersions decreased, and led to the drop in the gel strength according to volume blocking mechanism of hard-sphere theory. As temperature increased above the VPTTs of PIB nanogels, the enhanced inter-particle forces (hydrophobic interaction and electrostatic force) resulted in the increasing of G' and G" value. Compared with 4 wt% and 5 wt% of PIB nanogel dispersions, the gold nanoparticles in HCC431 dispersions enhanced further G' and G" value of shrunken gel phase.

In addition to the gel strength in blood-vessel embolizaiton, the injection flowability played important role on the clinical use of embolic materials. Figure 6B showed the curves about the viscosity *vs* shear rate of HCC and PIB nanogel dispersions at flowable sol phase. All of dispersions including HCC and PIB nanogels showed a viscosity reduction with the increasing of shear rate. The so-called shearing-thinning effect was helpful to achieve better flowability for the injection of embolic materials. HCC431 dispersions exhibited excellent shearing-thinning effect. Compared with PIB nanogel dispersions, that is to say, HCC431 dispersions showed a higher viscosity at lower shear rate, and a lower viscosity at higher shear rate.

The *in vivo* DSA angiography and blood-vessel embolizing evaluation

The *in vivo* embolization evaluation of HCC dispersions was performed using a digital subtracted angiography (DSA) in the renal artery of Japanese rabbits. The black shadow in Figure 7A was the DSA image of rabbit renal arteries by infusing a radiopaque agent, Omnipaque (300 mg I/mL), and it disappeared completely after embolized by HCC431 dispersions as shown at the red arrow in Figure 7B. This indicated clearly that HCC431 dispersions exhibited the similar ability of blood-vessel embolization as Ivalon, one of the most common embolic-agent in clinic (Figure 7C and 7D). It was worth noting that HCC431 dispersions showed a more clear shadow (the red arrow in Figure 7B) than Ivalon (the red arrow in Figure 7D), and higher solution in angiographic image than Omnipaque (the white arrow in Figure 7B and 7D). These *in vivo* results indicated that HCC431 dispersions showed both high angiographic ability and good blood-vessel embolization, and could be used to postoperative examination for long periods owing to the entrapment of GNPs into the embolic sites by the gellating of PIB nanogel dispersion.

It is well known that permanent embolization to blood-vessel is essential in TAE therapy for preventing vascular recanalization under blood scouring. Figure 8 showed that the angiography and histopathology evaluations in the permanent embolization to rabbit renal arteries with HCC431 dispersions. The black shadow in Figure 8A, which reflected renal arteries, has disappeared in Figure 8B, 8C and 8D. It indicated that the renal arteries were successfully embolized by HCC431 disperisons. Moreover, vascular recanalization was not found after the embolization of HCC431 dispersions for 28 d. In contrast to the rabbit kidney with normal structures in the histological section of Figure 8A, coagulative necrosis appeared after embolized by HCC431 dispersions for 3d, and only the residual shadows of kidney tubules and glomeruli was found in the histological section of Figure 8B. In that of Figure 8C, large necrotic regions were found in kidney tissues, and the outlines of kindey tubules and glomeruli became vague after the embolization of HCC431 dispersions for 7d. The large necrotic regions were also found after the embolization of HCC431 dispersions for 14d, and the calcifications of some kidney tubules and glomeruli were observed in the histological section of Figure 8D. When the kidney tissues were ebmolized by HCC431 dispersions for 28d, extensive fibrosis and calcification appeared in the histological section of Figure 8E. It indicated that HCC431 dispersions could effectively cut off the blood supply of kidney over a long period, and lead to coagulative necrosis of kidney tissues.

Biocompability evaluation of HCC dispersions

Biocompability was paid extensive attention for the potential application of new biomaterials in clinic. Au NPs and PNIPAM polymers exhibited good biosafety either *in vivo* and/or *in vitro* as previously reported.[11-15] In Figure 9A, the cytotoxic results indicated that the L929 cell viability was higher than 85%, no

significant difference between PIB nanogels and HCC dispersions. Moreover, the hemolysis ratios of three groups (PIB nanogels, HCC431 and HCC531) were lower than 3.0% (Figure 9B). The hemolysis results indicated that HCC dispersions had good blood-compatibility. Figure 9C and 9D showed the hepatic and renal functions of normal rabbits under renal artery embolization. Alanine aminotransferase (ALT) and aspartate aminotransferase (AST) levels, which reflected hepatic function, slightly increased at 1d post embolization of HCC dispersions. However, The ALT and AST levels quickly decreased to normal levels at 3d post-embolization. Blood urea nitrogen (BUN) and creatinine (CRE) levels, which reflected renal function, sharply increased respectively to 21.3 ± 4.8 and 253.8 ± 43.8 μmol/L at 1 d post-embolization, and decreased to normal levels (about 9.8 ± 3.6 and 102.8 ± 18.5 μmol/L, respectively) at 14 d post-embolization. These results indicated that HCC dispersions had good histocompatibility, although they had a transitory effect on hepatorenal function at 1-3 d post-embolization.

Conclusions

In order to resolve the drawbacks of iodine-based X-ray contrast agents in the blood-vessel embolization therapy of tumor, in the present work, high concentrated complex (HCC) dispersions between temperature sensitive nanogels and GNPs were developed as new blood-vessel-embolic materials with high-resolution angiography. Owing to good dispersion stability of the GNPs in HCC dispersions, which were characterized by UV/Vis spectrophotometer and electron microscopes (SEM and TEM), HCC dispersions showed excellent X-ray attenuation ability which was 2.6 times at 0.31 mmol Au or I/mL. In the two sol-gel transitions temperature ($T_{g\text{-}s}$ and $T'_{s\text{-}g}$) of PIB nanogel dispersions, GNPs had no influence on the $T'_{s\text{-}g}$ values, and great influence on the $T_{g\text{-}s}$ values of HCC dispersions. The animal data indicated that HCC dispersions showed both high angiographic ability and good blood-vessel embolization, and could be used to postoperative examination for long periods owing to the entrapment of GNPs into the embolic sites by the gellating of PIB nanogel dispersion. The HCC dispersions are hopeful to be developed as new blood-vessel-embolic materials with high-resolution angiography.

Acknowledgements

This work was financially supported by National Basic Research Program of China (973 Program, 2012CB932500), the Fundamental Research Funds for the Central Universities (2014TS088) and National Basic Research Program of China (SS2012AA023804). We give thanks to the analysis and Test Center of Huazhong University of Science and Technology for the related analysis. Jiangshan Wan, Kun Qian and Yingying Ma contributed equally to this work.

Notes and references

[a] *National Engineering Research Center for Nanomedicine, Huazhong University of Science and Technology, 430074, Wuhan City, P. R. China. Fax: 86 27 87792234; Tel: 86 27 87792234; E-mail: zhaoyb@hust.edu.cn*

[b] *Interventional Radiology Department of Wuhan Union Hospital, Huazhong University of Science and Technology, 430022, Wuhan City, P. R. China.Fax: 86 27 85726432; Tel: 86 27 85726807; E-mail: hqzcsxh@sina.com*

† Electronic Supplementary Information (ESI) available: [details of any supplementary information available should be included here]. See DOI: 10.1039/b000000x/

‡ Footnotes should appear here. These might include comments relevant to but not central to the matter under discussion, limited experimental and spectral data, and crystallographic data.

1 R. J. Lewandowski, J. F. Geschwind, E. Liapi, R. Salem, *Radiology*, 2011, 259, 641
2 H. Zhao, C. S. Zheng, Y. B. Zhao, H. Liang, H. Wu, G. F. Zhou, B. Liang, Y. Wang, X. Xia, *Am. J. Neuroradiol.* 2013, 34, 169
3 K. Saralidze, M. L. W. Knetsch, C. van der Marel, L. H. Koole, *Biomacromolecules* 2012, 11, 3556
4 C. S. J. van Hooy-Corstjens, K. Saralidze, M. L. W. Knetsch, P. J. Emans, M. W. de Haan, P. C. M. M. Magusin, B. Mezari, L. H. Koole, *Biomacromolecules* 2008, 9, 84
5 D. Mawad, A. Lauto, A. Penciu, H. Mehier, B. Fenet, H. Fessi, Y. Chevalier, *Nanotechnology* 2010, 21, 335603
6 P. E. Le Renard, O. Jordan, A. Faes, A. P. Fink, H. Hofmann, D. Rufenacht, F. Bosman, F. Buchegger, E. Doelker, *Biomaterials* 2010, 31, 6915
7 X. L. Lv, Z. X. Wu, C. H. Jiang, Y. X. Li, X. J. Yang, Y. P. Zhang, N. Zhang, *Eur. J. Radiol.* 2011, 80, 776
8 I. B. Maribel, S. P. Walsh, Z. Schwartz, B. D. Boyan, *J. Biomed. Mater. Res. Part B* 2012, 100B, 1451
9 D. F. M. Carli, M. Sluzewski, G. N. Beute, W. J. van Rooij, *Am. J. Neuroradiol.* 2010, 31, 152
10 B. Guiu, F. Deschamps, S. Aho, F. Munck, C. Dromain, V. Boige, D. Malka, S. Leboulleux, M. Ducreux, M. Schlumberger, *J. Hepatol.* 2012, 56, 609
11 Y. B. Zhao, C. S. Zheng, Q. Wang, J. L. Fang, G. F. Zhou, H. Zhao, Y. J. Yang, H. B. Xu, G. S. Feng, X. L. Yang, *Adv. Funct. Mater.* 2011, 21, 2035
12 K. Saha, S. S. Agasti, C. Kim, X. N. Li, V. M. Rotello, *Chem. Rev.* 2012, 112, 2739
13 A. J. Mieszawska, W. J. M. Mulder, Z. A. Fayad, D. P. Cormode, *Mol. Pharm.* 2013, 10, 831
14 A. Jakhmola, N. Anton, T. F. Vandamme, *Adv. Healthc. Mater.* 2012, 1, 413
15 Y. Liu, K. Ai, L. Lu, *Accounts Chem. Res.* 2012, 45, 1817
16 N. Lee, S. H. Choi, T. Hyeon, *Adv. Mater.* 2013, 25, 2641
17 C. J. Xu, G. A. Tung, S. H. Sun. *Chem. Mat.* 2008, 20, 4167
18 R. Guo, H. Wang, C. Peng, M. W. Shen, M. J. Pan, X. Y. Cao, G. X. Zhang, X. Y. Shi, *J. Phys. Chem. C* 2010, 114, 50
19 D. Kim, S. Park, J. H. Lee, Y. Y. Jeong, S. Y. Jon, *J. Am. Chem. Soc.* 2007, 129, 7661
20 H. Wang, L. F. Zheng, R. Guo, C. Peng, M. W. Shen, X. Y. Shi, G. X. Zhang, *Nanoscale Res. Lett.* 2012, 7, 190
21 Q. Yin, F. Y. Yap, L. C. Yin, L. Ma, Q. Zhou, L. W. Dobrucki, T. M. Fan, R. C. Gaba, J. J. Cheng, *J. Am. Chem. Soc.* 2013, 135, 13620
22 A. de Vries, E. Custers, J. Lub, S. van den Bosch, K. Nicolay, H. Grull, *Biomaterials* 2010, 31, 6537
23 Jiali Niu, Tao Zhu, Zhongfan Liu, *Nanotechnology*, 2007, 18, 325607
24 Y. Y. Ma, J. Zeng, W. Y. Li, M. McKiernan, Z. X. Xie, Y. N. Xia, *Adv. Mater.* 2010, 22, 1930
25 M. Destribats, V. Lapeyre, M. Wolfs, E. Sellier, F. L. Calderon, V. Ravaine, V. Schmitt, *Soft Matter* 2011, 7, 7689
26 C. G. de Kruif, E. M. F. van Iersel, A. Vrij, W. B. Russel, *J. Chem. Phys.* 1985, 83, 4717
27 D. M. Ole Kiminta, P. F. Luckham, S. Lenon, *Polymer* 1995, 36, 4827

Cite this: DOI: 10.1039/c0xx00000x

www.rsc.org/xxxxxx

ARTICLE TYPE

Captions:

Figure 1. The characterization of gold nanoparticles: (A) TEM images; (B) X-ray powderdiffraction (XRD)

Figure 2. The zeta potential of PIB nanogels with temperature. The inset plot was TEM photographs of PIB nanogels, the scale was 200 nm

Figure 3 The stability of gold nanoparticle dispersions: Plot A was the UV/Vis spectra comparison of cGNP and HCC431 dispersions. The black line and red line were cGNP dispersions (0.04 mol/L) before and after lyohilization and redispersion in water, respectively. The blue line was HCC431dispersions. The inset photographs was the lyophilized powder of cGNP and HCC431 dispersions; Plot B and Plot C were the photographs of cGNP and HCC431 dispersions prepared with the processes of lyohilization and redispersion, respectively. Plot D_1 and D_2 were the SEM photographs of PIB nanogels (4 wt%) and HCC431 dispersions, respectively. The scale was 5 μm. Plot D_3 and D_4 were the SEM photographs of cGNP dispersions and HCC431 dispersions, respectively. The scale was 200 nm.

Figure 4. The X-ray attenuation of HCC dispersions (solid sphere) compared with Omipaque (hollow square) as a function of gold or iodine concentration measured using a CT scanner (A) and an IVIS Lumina XR system (B).

Figure 5. The sol-gel phase transition diagrams of HCC dispersions. (A) The phase diagram of temperature *vs* nanogel concentration. The gold content in HCC dispersions was 0.31 mol/L; (B) the phase diagram of temperature *vs* gold content. The nanogel concentration in HCCs was 4 wt%

Figure 6. (A) The dynamic viscoelastic comparision of HCC431 dispersions (red) with 4 wt% (green) of PIB nanogel dispersions. Storage modulus (G', solid spheres), loss modulus (G'', hollow spheres); (B) The shearing-thinning effect of HCC431 (red) and 4 wt% of PIB nanogel dispersions (green)

Figure 7. The angiographic comparison of *in vivo* embolization using HCC431 and Ivalon. Plot A and B were the DSA images before and after embolization of HCC431, respectively. In plot B, the black shadow (at the red arrow) was the region of renal artery embolized by HCC431, and the gray shadow (at the white arrow) was the region of renal artery infused by Omnipaque. Plot C and D were the DSA images before and after embolization of Ivalon, respectively. In plot D, the black shadow (at the red arrow) was the region of renal artery embolized by Ivalon, and the gray shadow (at the white arrow) was the region of renal artery infused by Omnipaque.

Figure 8. The permanent embolization evaluations to rabbit renal arteries with HCC431 dispersions: (A), (B), (C), (D) and (E) were the DSA images and histological sections (HE × 100) prior to blood-vessel embolization, 3d, 7d, 14d and 28d post-embolization of HCC431 dispersions, respectively.

Figure 9. Biocompatibility evaluation of HCC dispersions: (A) The cytotoxicity evaluation to L929 cells by CCK-8 method (n = 6); (B) The hemolysis evaluation (n = 10); (C) Alanine aminotransferase (ALT) and aspartate aminotransferase (AST) levels of normal rabbits after renal artery embolization with HCC431 dispersions; Blood urea nitrogen (BUN) and creatinine (CRE) levels of normal rabbits after renal artery embolization with HCC431 dispersions (n=10).

Table 1. the nanogel concentrations and gold contents of various HCC disperisons

	HCC409	HCC509	HCC431	HCC531
Nanogel powder, g	0.040	0.050	0.040	0.050
cGNP dispersion, mL	2	2	7	7
Nanogel content, wt%	4.0	5.0	4.0	5.0
Gold content, mol/L	0.09	0.09	0.31	0.31

Figure 1.

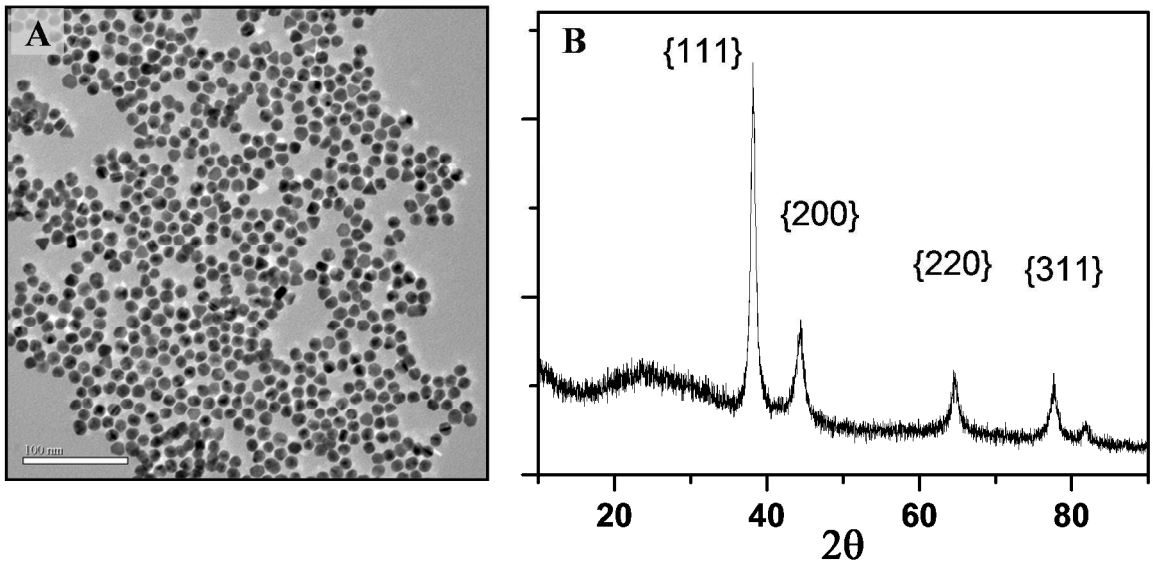

Figure 2.

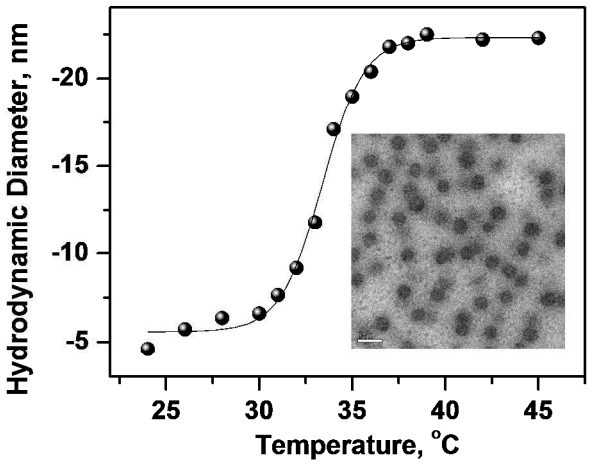

Figure 3

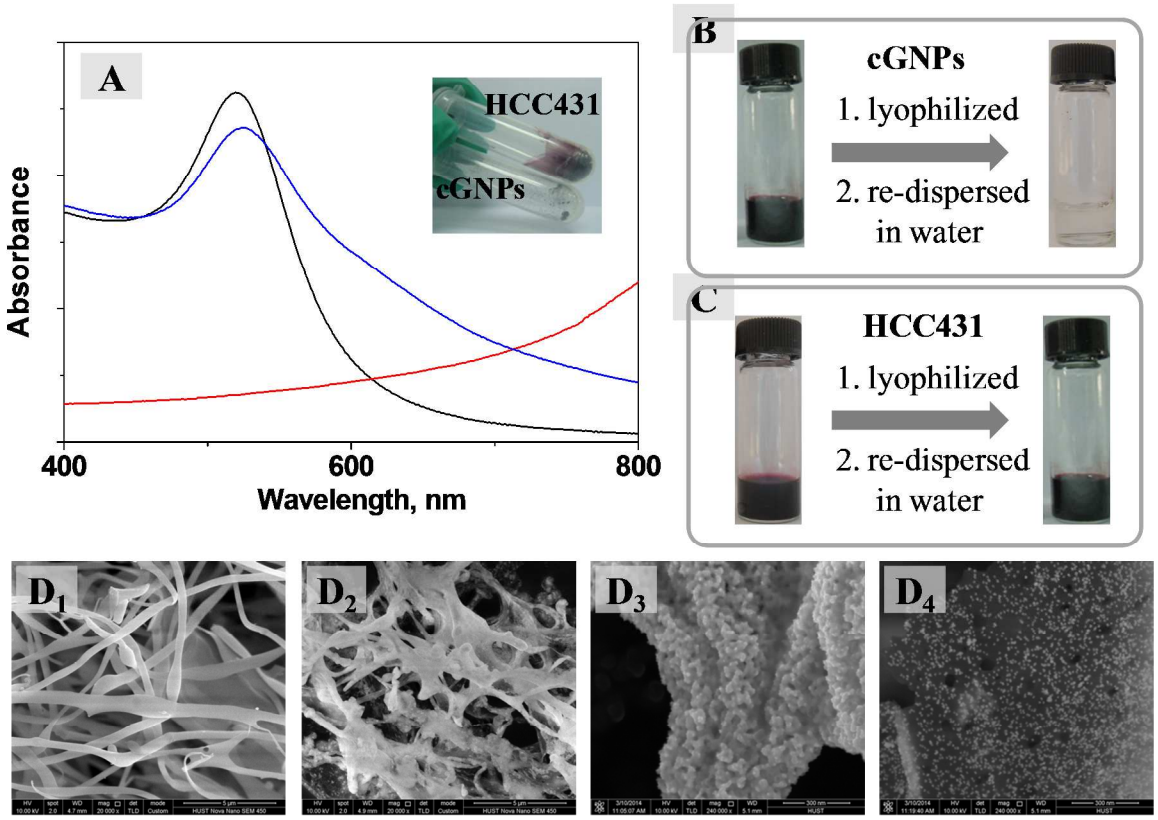

Figure 4.

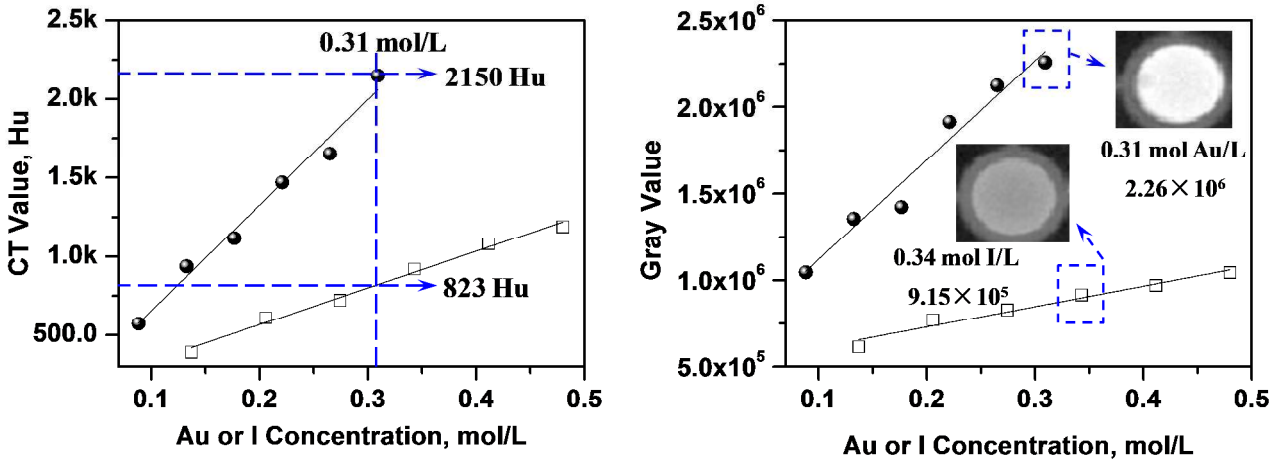

Figure 5.

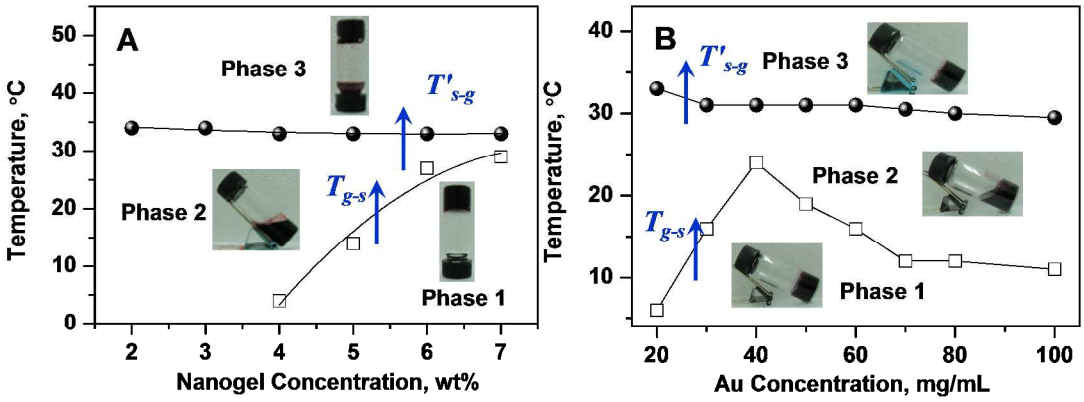

Figure 6.

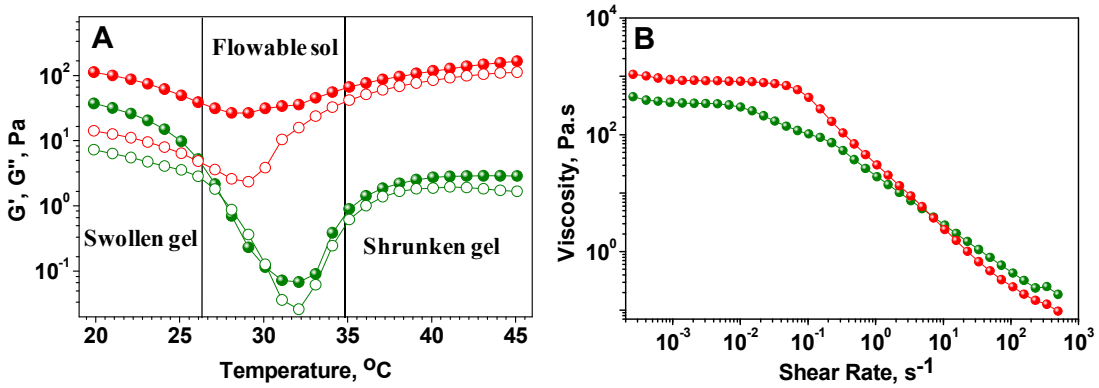

Figure 7.

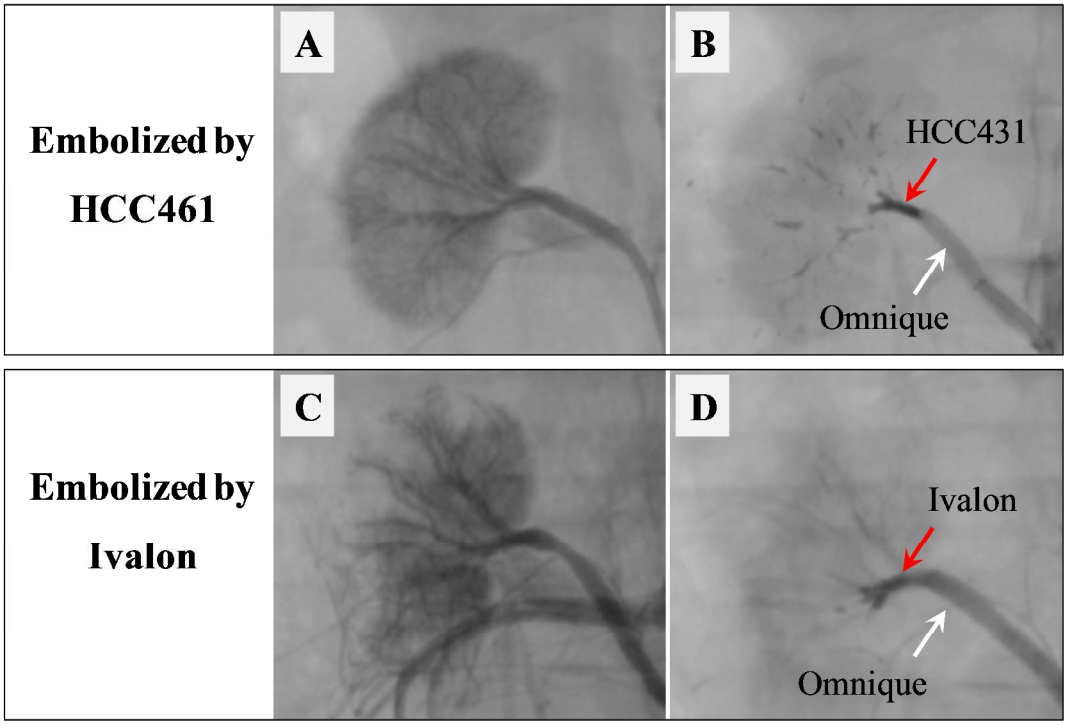

Figure 8

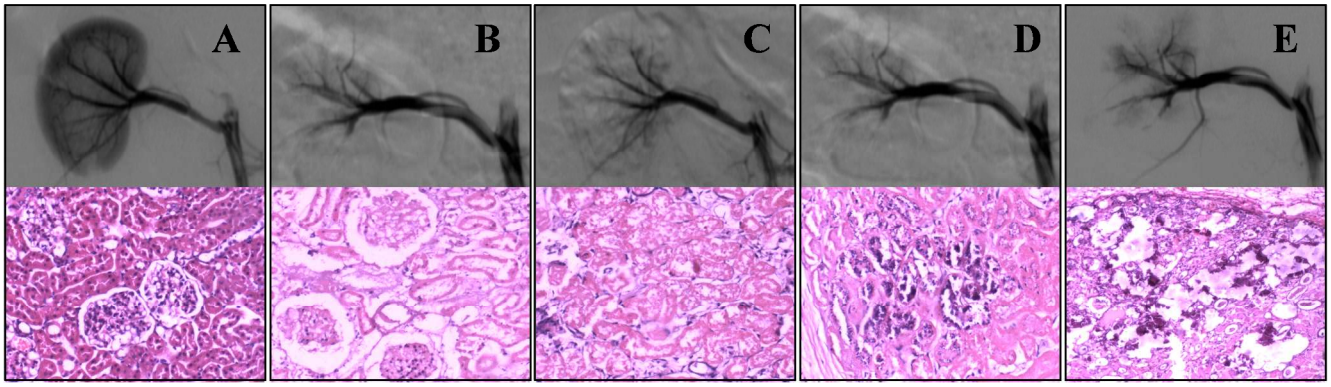

Figure 9

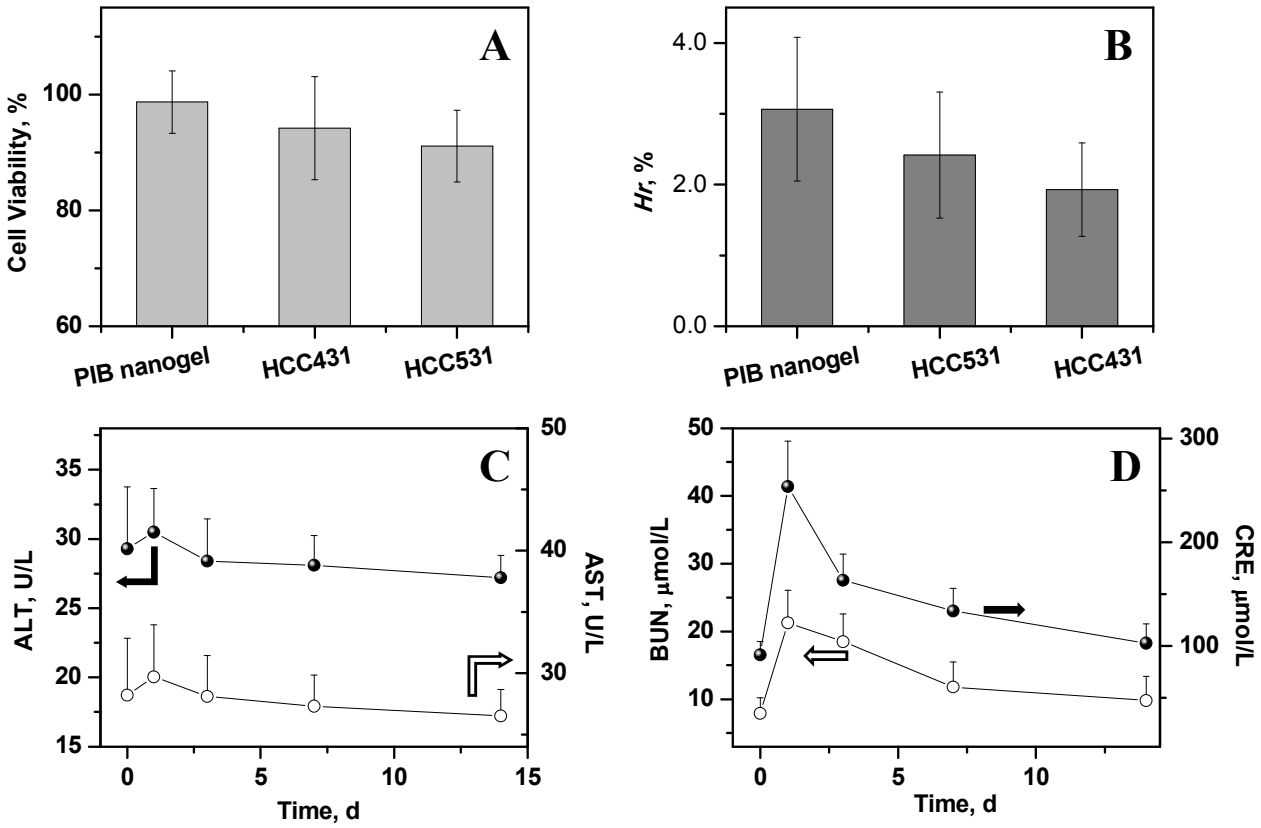

5

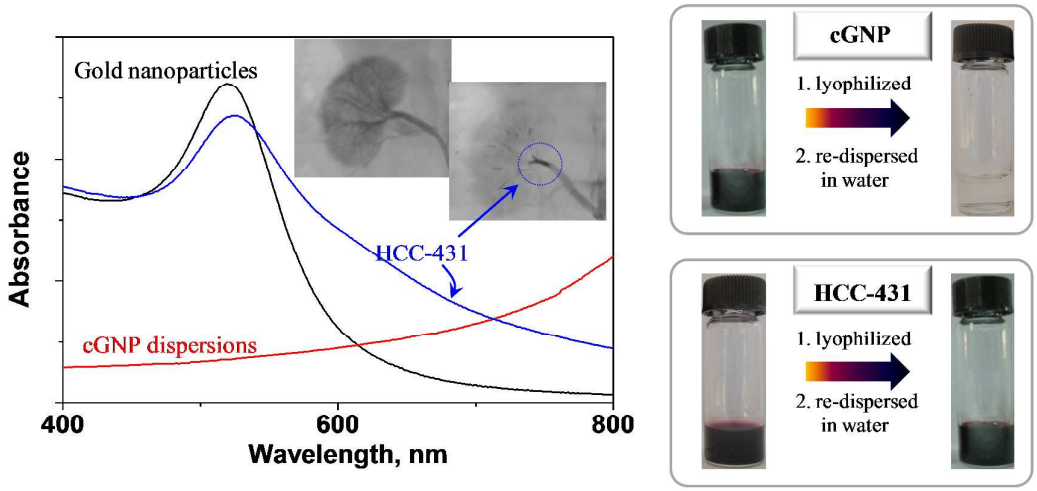

The poor stability of gold nanoparticles at high concentration limited its application as blood-pool contrast agent. In order to improve their colloid stability, a facile method were developed by mixing gold nanoparticles with p(*N*-isopropylacrylamide-*co*-butyl methylacrylate) (PIB) nanogels. The resulting high concentrated complex (HCC) dispersions effectively inhibited the aggregation of gold nanoparticles, and then exhibited better ability in blood-pool imaging than Omipaque, a commercial iodinated contrast agent. Meanwhile, the blood-vessel embolization of temperature sensitive PIB nanogels was improved owing to the replacement of iodinated compound with gold nanoparticles. The HCC dispersions are hopeful to be developed as novel interventional diagnosis and therapy materials of blood-pool imaging and blood-vessel embolizing properties